New in-situ techniques for measuring the properties of root-reinforced soil – Laboratory evaluation

G. J. Meijer[*†‡§] A. G. Bengough[*†] J. A. Knappett[*] K. W. Loades[†]
B. C. Nicoll[‡]

Published in: Géotechnique 66(1), 27–40 (2016). DOI:10.1680/jgeot.15.P.060

Abstract

Mechanical root-reinforcement is one of the mechanisms by which vegetation enhances slope stability. Common approaches to quantify this effect include either in-situ shear box testing or destructive root sampling combined with a theoretical model to estimate reinforcement parameters. Both approaches however are time consuming. Here we evaluate four new in-situ techniques to quantify mechanical root-reinforcement and compare these under laboratory conditions. All four methods yield distinct results in soils reinforced with woody root analogues (ABS rods), fine root analogues (polypropylene fibres) or stones. Two methods (adaptations of penetrometer testing, dubbed 'blade penetrometer' and 'pull-up') are suitable for spatially locating rooted zones and individual roots, while the other two ('pin vane' and 'cork screw' extraction) demonstrate potential for directly quantifying the rooted soil stress-strain behaviour. These simple methods are suitable for use on difficult to access terrain where many measurements are needed to quantify spatial and temporal variability of root-zone properties for geotechnical calculations. The techniques are quicker to use than conventional methods and so should improve the reliability of slope stability predictions.

KEYWORDS: in situ testing; slopes; vegetation

1 Introduction

Vegetation can be a sustainable and cost-effective way to stabilise slopes (Coppin and Richards, 1990; Gray and Sotir, 1996; Norris et al., 2008; Stokes et al., 2008, 2009). Roots are known to affect soil strength in various ways. Mechanical reinforcement is derived from fine roots acting as tensile reinforcement or thicker roots acting similarly to soil nails in bending (Gray and Sotir, 1996). Roots affect soil hydrology by reducing water content by evapotranspiration and increasing soil permeability (Collison et al., 1995; Gray and Sotir, 1996; Kim et al., 2013). Plant root mucilage, combined with wetting and drying cycles, affects soil structure generation in the rhizosphere soil around the roots (Pohl et al., 2009; Fattet et al., 2011).

[*]University of Dundee, Division of Civil Engineering, Dundee DD1 4HN, UK
[†]James Hutton Institute, Invergowrie, Dundee DD2 5DA, UK
[‡]Forest Research, Northern Research Station, Roslin, Midlothian EH25 9SY, UK
[§]Corresponding author, g.j.z.meijer@dundee.ac.uk

Landslide risk often coincides with periods of heavy or prolonged rainfall, so hydrological reinforcement will be smallest when most needed (Pollen-Bankhead and Simon, 2010). The mechanical reinforcement introduced by fine roots, often classified as roots smaller than 2 mm (Wang et al., 2006; Achat et al., 2008; Stokes et al., 2009), is often considered to be most important (Coppin and Richards, 1990), due to large quantities of thin roots of high root tensile strength present.

One commonly adopted strategy to quantify root reinforcement is to measure root quantity, diameter and tensile strength and convert this data into an additional soil cohesion term ('root cohesion' c_r). The simple Wu/Waldron Model (WWM) can be used (e.g. Wu et al., 1979), but generally overestimates reinforcement (e.g. Loades et al., 2010). Fibre Bundle models (FBM) are more accurate, taking sequential root breakage into account (e.g. Pollen and Simon, 2005). A third class of models, although less commonly used, take soil-root interaction into account using spring models. Roots are modelled as spring-supported laterally loaded piles, taking into account root bending (e.g. Wu and Watson, 1998; Duckett, 2014). All three classes of models require time consuming field sampling to measure the root properties in the laboratory.

Another strategy to quantify reinforcement is directly measuring reinforced shear strength in-situ. The most common test uses a field shear box. Various designs have been proposed (Wu et al., 1979; Endo, 1980; Hengchaovanich and Nilaweera, 1996; Ekanayake et al., 1997; Wu and Watson, 1998; Norris and Greenwood, 2003; Cammeraat et al., 2005; Docker and Hubble, 2008; Fan and Su, 2008; Comino et al., 2010). There is no standard for conducting this test, and a wide variety in shear box size (usually with a shear plane between 30×30 and 60×60 cm), depth, shear rate, test control (force- or displacement controlled), hydrological conditions (saturated, field capacity) and overburden pressure is reported. These tests are also time-consuming and require heavy equipment, making them less suitable to apply on difficult terrain.

Quantifying root-reinforcement on slopes is further complicated by spatial variability in root characteristics, architecture, soil type, soil strength and hydrology, resulting in the need for large numbers of measurements. Spatial variability is often neglected in root-reinforced slope stability assessments, but might be very important as landslides will localise in weaker zones. Several investigations have been made to take variation in root quantity into account (Genet et al., 2008; Pollen-Bankhead and Simon, 2009; Schwarz et al., 2010; Mao et al., 2013, 2014), although often only localised variation is measured and then applied to the whole slope. Root-reinforced stress-strain behaviour needs to be studied in more detail. During landslide initialisation, soil shear strains vary along the sliding surface because of progressive failure. Use of only peak strengths in stability analyses leads to overestimations of slope safety. When dealing with root-reinforcement, this might be even more important, as the difference between peak and residual strength will be larger due to root breakage. This spatial mobilisation of roots is neglected assuming root-reinforcement acts merely as an increase in global cohesion.

Because of the limitations of existing methodologies, there is a need for a quick (allowing more tests in a given time), simple (for inaccessible sites) and robust (applicable in various root and soil conditions) method to accurately quantify mechanical root reinforcement. This paper introduces four devices and compares their relative performance using laboratory testing in repacked field soil containing root analogues. Device performance is also compared in

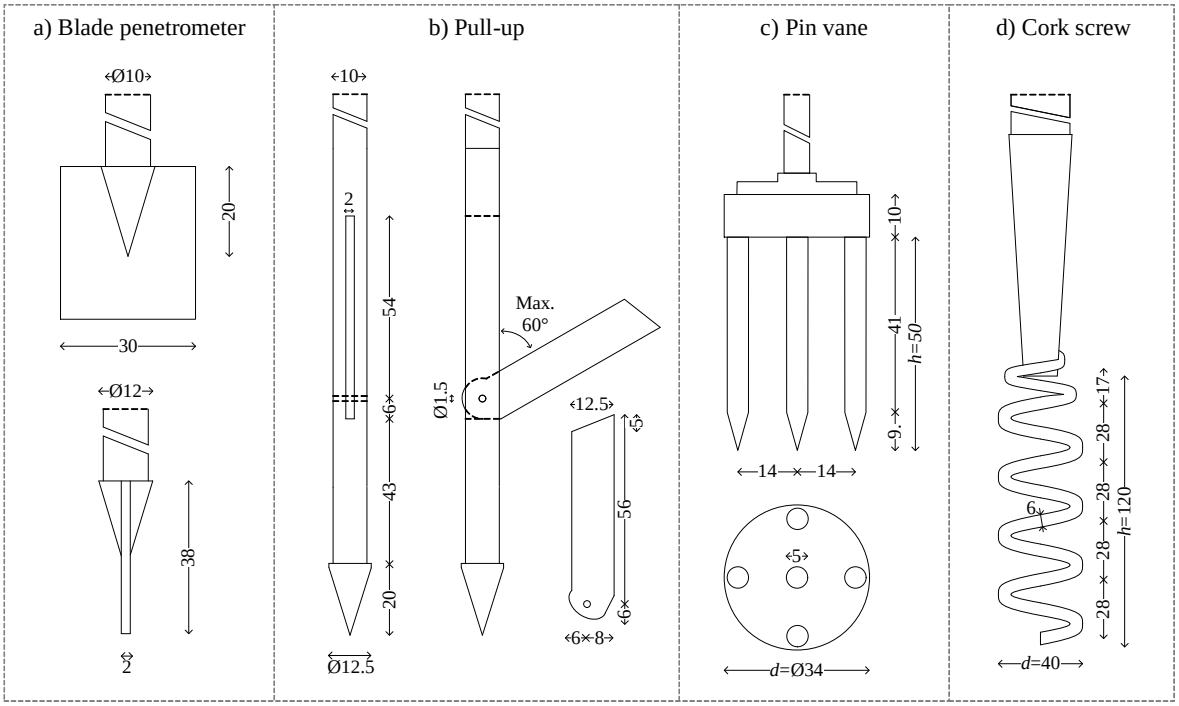

Figure 1: Technical drawings of the four devices: (a) blade penetrometer; (b) pull-up; (c) pin vane; (d) corkscrew. All dimensions are in mm

fallow soil and in soil containing additional stony layers.

2 Methods

2.1 Proposed devices

In the following sections four new potential measurement devices (Figure 1) are introduced and discussed. One of the major design criteria was the sensitivity of the measurements for detecting forces associated with the presence of roots.

Blade penetrometer method: In standard penetrometer tests, cone resistance is correlated with soil strength and type, but it is unclear if this is the same for rooted soil. However, a distinction between the behaviour of relatively thick individual roots and the behaviour of a dense, fine root network must be made.

Individual roots will be strained when pushed down by the blade penetrometer until breakage or slippage of a root end from the surrounding soil. Failure may be visible in the resistance profile as a distinct resistance peak at the root depth. This is similar to root pull-out test readings, where main root or side branch failure can be observed from the force-displacement plots (Riestenberg, 1994; Norris, 2005; Docker and Hubble, 2008; Giadrossich et al., 2013). The characteristics of these peaks (magnitude, slope) can be related to root properties such as diameter and strength. A model, for example spring-supported laterally loaded pile theory, can then be used to obtain these properties. Subsequently, these can be used to determine root reinforcement using any of the models described earlier, e.g. the WWM, FBM or numerical models.

Densely fine rooted soil on the other hand will likely behave as a composite material. The

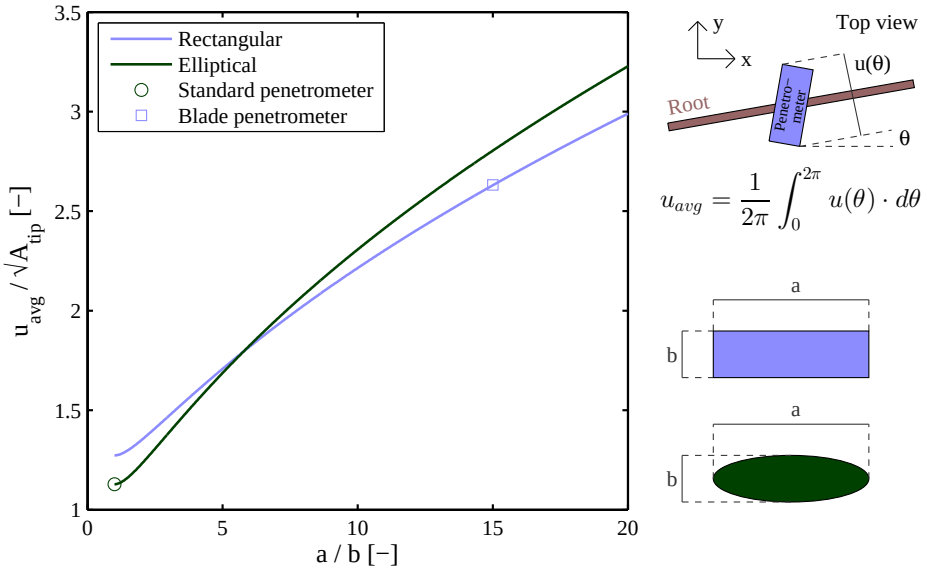

Figure 2: Sensitivity for one-dimensional object detection for rectangular and ellipsoid penetrometer tip shapes.

effect of an individual fine root between many others might be indistinguishable. A general increase in resistance over a large soil strain range is expected, similar to the observed increase in peak and residual shear strength in fibre-reinforced sands measured with triaxial, direct shear or ring shear tests (Gray and Ohashi, 1983; Jewell and Wroth, 1987; Michalowski and Çermák, 2002; Heineck et al., 2005; Ibraim and Fourmont, 2007; Tang et al., 2007; Diambra et al., 2010). In this case empirical relations between the depth-resistance trace and rooted soil shear strength are required.

A penetrometer fitted with an elongated tip increases sensitivity for measuring root effects. This can be understood by simplifying roots to 1-dimensional line objects. For a single root with azimuth θ, the chance it will be hit by the penetrometer is proportional to the projected width (u) of the penetrometer in the transverse direction to the root:

$$u(\theta) = \max\left(y_i \cos\theta - x_i \sin\theta\right) - min(y_i \cos\theta - x_i \sin\theta) \tag{1}$$

where (x_i,y_i) are the coordinates of any point i in the horizontal cross section of the penetrometer (Figure 2). When the root azimuths are assumed to be uniformly distributed, the chance a penetrometer hits a root is proportional to the 'average' width of the tip (u_{avg}):

$$u_{avg} = \frac{1}{2\pi}\int_0^{2\pi} u(\theta) d\theta \tag{2}$$

When soil resistance is assumed to be proportional to tip area A_{tip}, the relative sensitivity to roots can be expressed in dimensionless terms as the ratio between u_{avg} and $\sqrt{A_{tip}}$ see Figure 2. This figure shows that the sensitivity is much larger for oblong shapes, and that the ratio of the major to the minor dimension is more important than the shape (rectangular or ellipsoidal). Although this simplified analysis does not take soil friction or tip shape effects into account, it clearly indicates the advantages of adapting a penetrometer tip for root measurements. A second advantage of an elongated shape is the opportunity this offers

for studying root growth direction anisotropy by varying the plane of orientation of the penetrometer.

In this study, a rectangular 30 mm wide by 2 mm thick stainless steel tip was used, see Figure 1a. To ensure structural rigidity, the height was chosen as 35 mm. This 'blade' was welded to a 30° 12 mm diameter standard agricultural penetrometer tip and screwed to a ∅10 mm shaft.

Pull-up method: Similar root-reinforced penetration profiles as measured by a blade penetrometer can be obtained in upwards rather than downwards movement. To yield reliable results, soil and root disturbance during installation needs to be minimised. Here, a standard 30° 12 mm diameter agricultural cone penetrometer with a 10 mm diameter shaft is used. Once the maximum profile depth is reached, a 2 mm thick blade was exposed from a recess in the shaft, see Figure 1b. During extraction, (almost) all of the resistance will act on the expanded blade, whereas during installation the test was similar to standard penetrometer testing. The blade shape was designed in such a way that it facilitates automatic opening during upwards movement. However, here expansion was performed manually to ensure the blade was fully exposed prior to extraction.

The main benefit of measuring root resistance in upwards movement is the ability to use the overlying soil surface to apply reaction force as the device is being extracted. This reduces the need for a counterweight that is required for penetrometer insertion. Secondly, the installation phase yields a secondary set of data for the same soil profile but less influenced by roots, which might help to distinguish between fallow soil strength and root-reinforcement.

Pin vane method: Field vane devices are well established to measure soil undrained shear strength in cohesive soil. However, a major limitation to their use in root-reinforced soil is potential root breakage and soil disturbance during the installation phase, resulting in strength underestimation. These effects were observed during vane testing in fibrous peats (Landva, 1980). Therefore, in the proposed design vane blades are replaced by prongs, see Figure 1c. During installation, the roots can slide between the prongs without breaking. The unbroken roots passing through the shear plane will be mobilized during the subsequent rotational shearing phase, adding reinforcement. Care must be taken when choosing prong spacing ensuring sufficient lateral soil resistance when rotated, e.g. the whole soil cylinder rotates, otherwise local soil failure around individual prongs might occur rather than the typical cylindrical block failure in vane tests. On the other hand, the spacing should be wider than the diameter of the roots in the soil to be tested, otherwise roots cannot be trapped within the pins.

The device used in our tests consists of five 5 mm diameter stainless steel pins: one central and four equally spaced along the outer perimeter with a centre-to-centre distance of 14 mm to the central axis. Pins are 50 mm long with ends having 30° conical tips. Because of this design, the installation resistance might be interpreted using CPT theory to estimate fallow soil strength parameters. The corresponding 10.8% tip area ratio, the ratio between the volume of the device and the sheared soil block, is lower than the maximum value of 12% prescribed by the British Standard (BS 1377-9:1990). To make the device sufficiently rigid, the top of the pins are held in place using a 10 mm thick steel disc. Because of this disc, soil has to be excavated to just above the desired test depth prior to each test, to prevent root accumulation and soil compaction beneath the device. In the interpretation of the results, shear resistance is assumed to be present only along the sides and bottom of the 33 mm

diameter (d) and 50 mm high (h) shearing cylinder. The root-reinforced soil shear resistance τ_{pv} is calculated from the measured torque T by:

$$\tau_{pv} = \frac{12T}{\pi d^2(6h + d)} \tag{3}$$

Cork screw method: Similar to the pin vane device, the proposed cork screw device mobilises shear strength along a cylindrical interface. Forces are mobilised during upwards rather than rotational displacement. Rotational installation (similar to inserting a cork screw into a wine bottle) minimises soil disturbance; only soil and roots close to the path of the screw tip are likely to be affected. During translational extraction shear resistance along the outer sides of the cylinder of soil trapped within the screw is mobilised. This includes the effect of undisturbed roots passing through this interface. The root-reinforced soil shear resistance τcs is derived from the measured extraction force F when tensile forces on the bottom interface are neglected:

$$\tau_{cs} = \frac{F}{\pi h d} \tag{4}$$

The support the screw gives to the trapped cylinder must be sufficiently large that the cylinder of soil remains intact.

In our tests, a ∅40 mm (outer diameter) carbon steel cork screw weeder (De Wit, The Netherlands) was used, see Figure 1d. Prior to each test soil was excavated to a depth corresponding with the planned top level of the screw to prevent root accumulation near the top of the device.

2.2 Soil and root analogues

Root analogues and recompacted soil were used to minimise variability in the initial testing and facilitate inter- and intra-device comparison. Two different root analogues were used in testing.

Straight Acrylonitrile Butadiene Styrene (ABS) plastic rods with circular cross sections were used as an analogue material for relatively thicker roots (diameters 1 and 4 mm). Rods were printed using a rapid prototyper ('3D-printer'; Liang et al., 2014, 2015). The benefits of using ABS are twofold: it enables creating 'roots' with reproducible characteristics, and secondly, material characteristics are comparable to real roots (Figure 3). The tensile strength was comparable to the highest reported values for roots in literature. The Youngs modulus of ABS had the same order of magnitude as available data for tree roots, but was greater than values for other plants.

To model dense fibrous root systems, like those of grass, 35 mm long ∅0.1 mm Loksand^{TM} polypropylene (PP) crimped fibres were used, similar to those used by Diambra et al. (2010). The tensile strength is similar to values for real roots (Figure 3).

Sandy loam topsoil (58.5% sand, 32.0% silt, 9.5% clay, Atterberg limits $w_L = 32\%$ and $w_P = 23\%$) was collected from the South Bullion field at the James Hutton Institute (Dundee, UK; Mickovski et al. 2009). Particles with diameters > 5 mm were removed using a rotary sieve after sampling. The gravimetric water content after sampling averaged $w = 20\%$. Soil was air dried to $w = 10$–17%, sieved again (< 2 mm) and packed into PVC tubes (150 mm internal diameter × 400 mm long). To some tubes gravel of two sizes was added: ∅4–5 mm subrounded gravel (South Bullion field) and angular ∅10–30 mm broken road gravel.

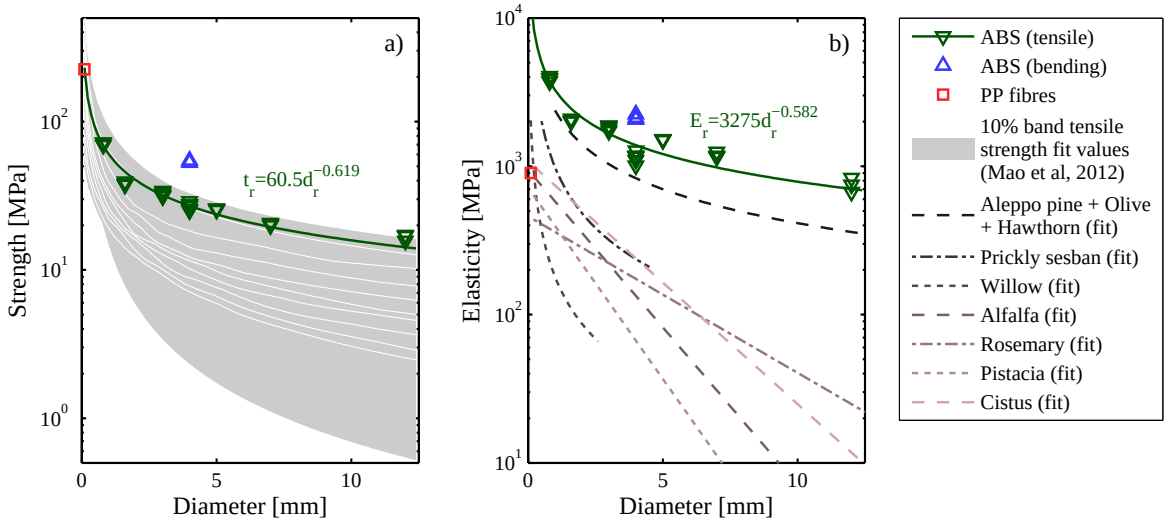

Figure 3: Comparison of (a) strengths and (b) Youngs moduli between root analogues and plant root data from the literature. In the strength plot, 40 fitted tensile strengthdiameter relationships for tree roots (Mao et al., 2012) are used to construct bands, each containing 10% of reported data. Data sources: ABS: present study; PP fibres: Diambra et al. (2010); Aleppo pine + olive + hawthorn: Van Beek et al. (2005); prickly sesban: Fan and Su (2008); willow, alfalfa, Pistacia and Cistus: Operstein and Frydman (2000).

2.3 Soil and root analogues

Soil was packed to a dry density of $\rho_d = 1.35$ Mgm^{-3} in 7 layers each with a thickness of 50 mm using a standard 2.5 kg Proctor hammer and a ∅150 mm hammering plate. The 5 mm wide outer rim of this plate protruded 5 mm to compact to a higher density around the edges and so discourage preferential water flow along the boundary during saturation and drainage. On average, 166.5 kJm^{-3} was applied to each layer (20 blows). Before adding a new layer, the top 5 mm of the previous layer was abraded to ensure layer bonding.

After compaction cores were saturated from the base in large plastic containers for 48 hours. During the first 24 h the water level was 150 mm below the soil surface. On the following day, this was raised to 20 mm above the soil surface. Full saturation was reached after approximately 36 h (confirmed by free water on top of the samples and theta probe measurements). Following saturation, cores were drained on sand tables to 1.5 kPa suction at their base. With a soil height of 350 mm in the core, this is equivalent to field conditions where the water table is 500 mm below the surface. All cores were drained for at least 4 full days to reach equilibrium (checked using mini tensiometers at the top of the core).

Water retention characteristics were determined using four samples packed in 100 cm^3 steel rings (average dry density $\rho_d = 1.34$ Mgm^{-3}). Samples were saturated for two days and subsequently equilibrated on ceramic plates (0.5, 1.0, 2.0, 5.0, 10, 20, 50 kPa suction). The corresponding results were fitted to the Van Genuchten model (Van Genuchten, 1980) in terms of saturations rather than volumetric or gravimetric water contents. Saturation is less sensitive to variations in soil dry densities:

$$S_r(s) = S_{r,r} + \frac{S_{r,s} - S_{s,s}}{\left(1 + (\alpha|s|)^n\right)^m} \tag{5}$$

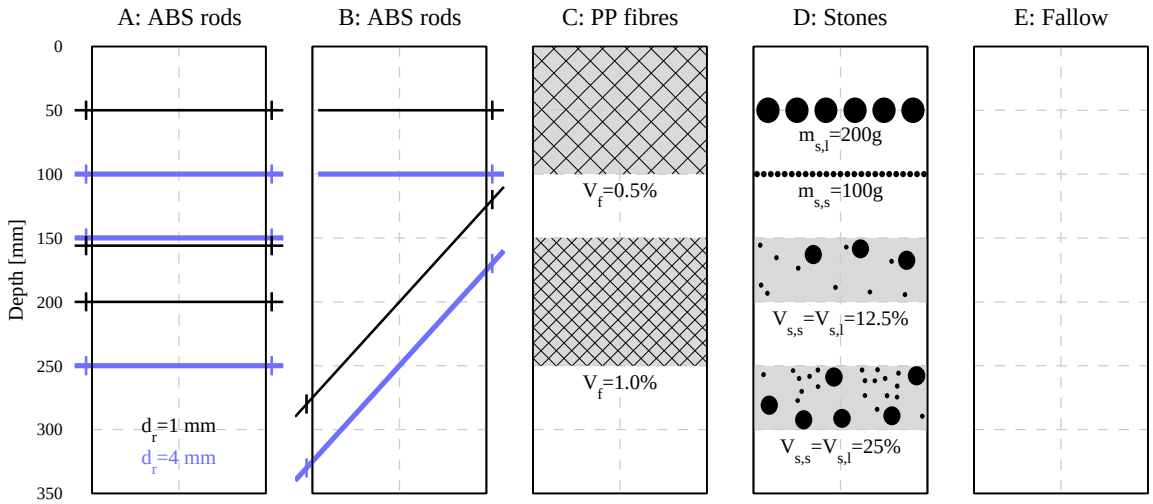

Figure 4: Schematic overview of soil and root test conditions used. In cores with fibres (case C) or stones (case D), quantities of fibres (V_f), small stones ($V_{s,s}$) and large stones ($V_{s,l}$) are expressed in volume fractions (%). Two layers a single stone thick are placed in the uppermost half of cores with stones. Of these, the total mass of stones (m_s) is given.

Where S_r is the saturation [%], s the suction level [kPa], $S_{r,s} = 100\%$ the saturation at saturated conditions (measured prior to testing), $S_{r,r}$=31.9% the residual saturation (fitted), and α, n and m dimensionless model parameters, fitted as 0.544, 1.333 and $(1 - 1/n)$ respectively ($R^2 = 98.9\%$). Based on these water retention parameters, saturations of $S_r = 77\%$ (top) to 91% (bottom) were expected in the soil cores.

Because of the limited size of the sand tables, 4–6 cores were prepared at a time ('batch'). Cores from the same batch were used for testing the same device in cores containing different inclusions (ABS, PP fibres, stones) rather than varying the device type and keeping the inclusion type constant. This choice was made to be better able to compare the behaviour of a single device between cores with various inclusions.

Dry bulk densities were measured using standard 100 cm^3 steel rings. Gravimetric water contents were determined using conventional oven drying (105°C). Measurements were corrected for the presence of stones, assuming a stone bulk density of 2.65 Mgm^{-3}.

For classification purposes and to check whether the adopted compaction method yielded a homogeneous soil, the strength of the soil was measured in two cores with no inclusions using a standard penetrometer (standard agricultural penetrometer, 30° ∅12 mm cone connected to a ∅10 mm shaft pushed at 300 mm min^{-1}) using an Instron 5966 universal testing machine.

2.4 Test conditions

Cores containing inclusions were made to test the various measurement devices under a range of conditions (Figure 4).

Cases A and B were prepared to study the behaviour of analogues of individual horizontal woody tree roots (∅1 mm and ∅4 mm). Many tree roots grow in (sub)horizontal direction, as tree roots explore the resource-rich topsoil layer (e.g. Reubens et al., 2007). In our testing straight root analogues were generally vertically spaced 50 mm apart so that root analogues would not affect each other (Figure 4). Therefore, in blade penetrometer, pull-up and vane

testing the effects could be studied individually. This was more difficult for cork screw tests because of the larger height of the device.

In *case A*, sections of horizontal thin (∅1 mm) and thicker (∅4 mm) roots were modelled using printed ABS. Translation was restricted at both rod ends by leading them through drilled holes in the side of the core and gluing a Perspex disc around the rod on the outside, preventing axial movement. This is intended to represent the tensile restraint on the ends of longer sections of root or short regions of branched roots. Individual rods were installed during packing when the soil level reached the level of the inclusion. At depth $z = 150$ mm, one ∅1 and ∅4 were placed 5 mm apart to see whether interactions of two individual roots occurs.

In *case B*, the top half of the core was used to model root ends with potential pull-out failure. When a root is loaded near its tip, reinforcement is expected to be lower as the root will slip at one end rather than break. In the bottom half, ABS rods were oriented at 45° to study the effect of root angle on the test results. Both ends of these angled rods were restrained and pushed in after the cores were filled to a level corresponding with the top end of the rod.

In *case C*, dense fibrous root mats were modelled using PP fibres. Two 100 mm thick rooted layers were modelled at different depths: one with a fibre volume fraction of 0.5% and the other, deeper layer, with 1.0% fibres. These percentages are in line with root fractions in the top layer (0–500 mm) found for tree species in Lombardy, Italy (Bischetti et al., 2005). Fibres and soil were premixed by hand in small quantities (1/70 of the total soil mass) until by visual examination the fibres were considered to be well-distributed (similar to Ibraim and Fourmont, 2007). Then the mixture was carefully deposited in the core. After each 10 batches, together forming one 50 mm thick core layer, the soil in the core was compacted as described earlier.

In *case D*, a stony soil was modelled. This was done for two reasons: firstly to study whether the developed methods can be reliably used in gravelly soil, and secondly to see whether gravel and roots yield distinct behaviour as both may be present in real soils. In the top half, for both size classes, a single layer of stones was manually deposited between two soil layers using 100 g (4–5 mm gravel) or 200 g (10–30 mm gravel) respectively. In the bottom half, two 50 mm thick stony soil layers were premixed with soil, carefully deposited in the core and compacted. Both contained equal volumes of both gravel size classes (assuming a density of $\rho = 2.65$ Mgm^{-3}). In the shallowest layer, the ratio of stone volume to total bulk volume equalled 12.5% and in the deeper layer 25% for each gravel size class. Different quantities are used in different layers to study the sensitivity of measurements to various amounts of stones.

Case E was a fallow soil sample, which served as control treatment.

2.5 Test set-up

Tests were performed using universal testing machines. For blade penetrometer, pull-up tests and CPT tests, an Instron 5966 fitted with a 2 kN load cell (Instron 2530-418) was used. For pin vane and cork screw testing, an Instron 4204 fitted with a 50 kN load cell (Instron 2525-802) was used. All Instron load cells are accurate to the maximum of either 0.25% of the indicated load or 0.025% of the maximum capacity. Forces and displacement were sampled at 20 Hz (Instron 4204) or 100 Hz (Instron 5966).

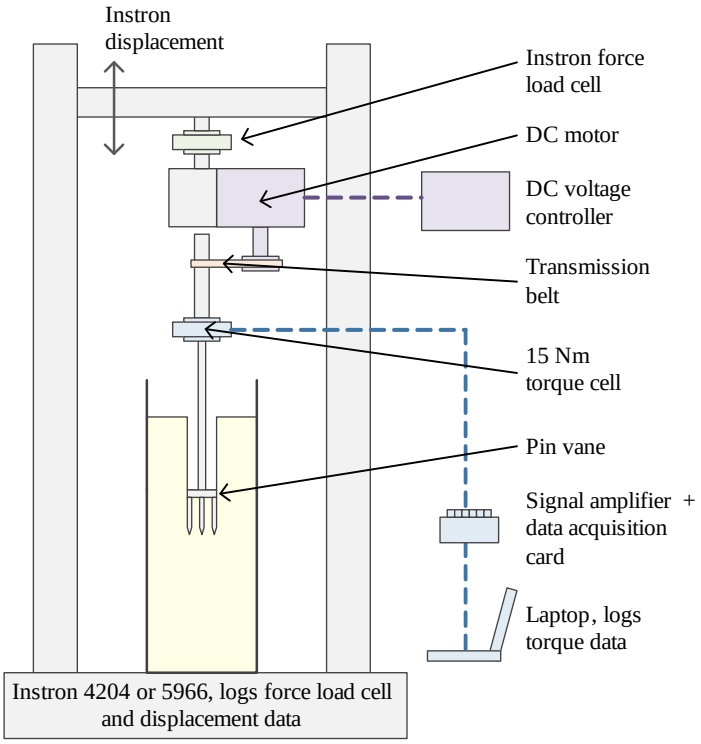

Figure 5: Schematic laboratory test set-up for pin vane (depicted) and corkscrew tests.

Table 1: Adopted displacement rates and corresponding test rates during the main shear test phase.

Test	Translation		Rotation	Test rate
	Downwards [mm min^{-1}]	Upwards [mm min^{-1}]	[r min^{-1}]	[ms^{-1}]
Blade penetrometer	300*	—	—	0.0050
Pull-up	300	300*	—	0.0050
Pin vane	300	—	4.43*	0.0025
Cork screw	116**	100*	4.23**	0.0017

* Main shear test phase

** Rates are linked based on cork screw pitch, to minimise soil disturbance during installation

The Instron 4204 set-up used a special rig to apply rotation (Figure 5). A DC shunt motor (Parvalux) was mounted in line with the shaft, the speed of which was controlled using a voltage regulator. Torque was measured using a 15 Nm load cell (Novatech F311-Z3862; sampling frequency 1000 Hz, resampled to 100 Hz by averaging every 10 measurements).

Displacement rates were chosen to reflect both expected application rates for in-situ use (Table 1) and typical shear displacements of landslides (Figure 6).

Test devices were inserted centrally at the top of the core. For pull-up tests, the cone was installed slightly off-centre so that the centre of the expanded wing coincided with the core central axis.

During blade penetrometer, pull-up and CPT tests, a single continuous measurement

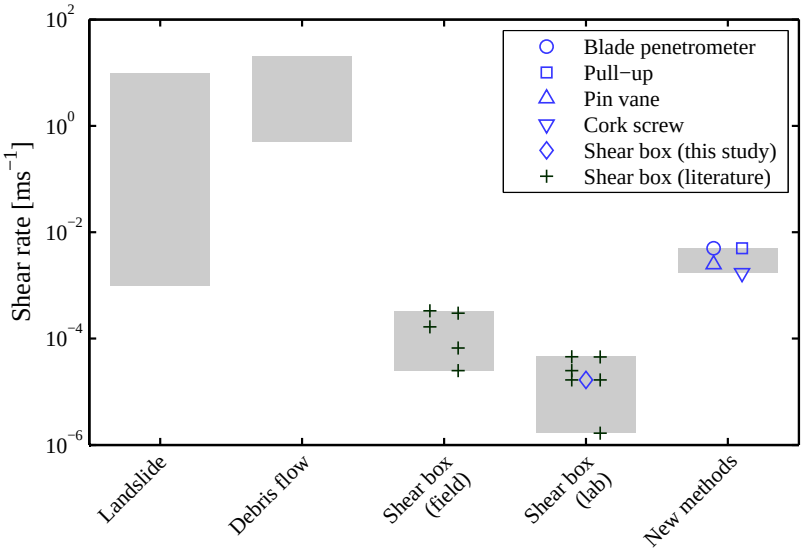

Figure 6: Typical shear rates for landslides and debris flows (Davies et al., 2010), field shear box testing (Ekanayake et al., 1997; Cammeraat et al., 2005; Docker and Hubble, 2008; Fan and Su, 2008; Mickovski et al., 2009, many other studies do not provide adopted rates), laboratory shear box testing on root-reinforced soil (Waldron, 1977; Waldron and Dakessian, 1981; Operstein and Frydman, 2000; Normaniza et al., 2008; Mickovski et al., 2009; Loades et al., 2010) and shear rates adopted in the present study.

profile was taken per core. In vane tests, measurements were taken every 50 mm between 25 and 325 mm depth (6 tests per core). In cork screw tests, measurements were taken at 0–125, 125–225 and 225–325 mm depths. Each pin vane or cork screw test was performed beneath the hole excavated during the previous test.

2.6 Reference shear tests

Direct shear tests were performed using a shear table custom built to shear the 150 mm cores (Mickovski et al. 2009, Figure 7). A load cell (Tedea Huntleigh 615, capacity 2 kN capacity, accuracy 1 N) was mounted between the screw jack and upper braces. Displacements were measured using a LVDT (RDP LDC6000C). Force and displacement were sampled at 10 Hz using a USB data acquisition unit (National Instruments USB-6008) and LabView software (National Instruments). All samples were sheared at a rate of 1 mm min^{-1}, in correspondence with root-reinforced soil shear box rates reported in the literature (Figure 6), until a maximum displacement of around 50 mm was reached. Equipment limitations did not allow faster shear rates.

The PVC pipes surrounding cores for shear box testing were cut at the appropriate depths and re-joined using tape before packing. To ensure water tightness, the seams were filled with petroleum jelly and the inside lined with a plastic sheet. The tape was removed before shearing, the top part of the core was slid approximately 3 mm vertically, maintaining a solid soil core, and the plastic lining cut with a scalpel blade.

Cores were sheared at various depths, see Figure 15. Most cores were prepared with fallow soil, although for the core types with PP fibres (case C) and stones (case D) a single core

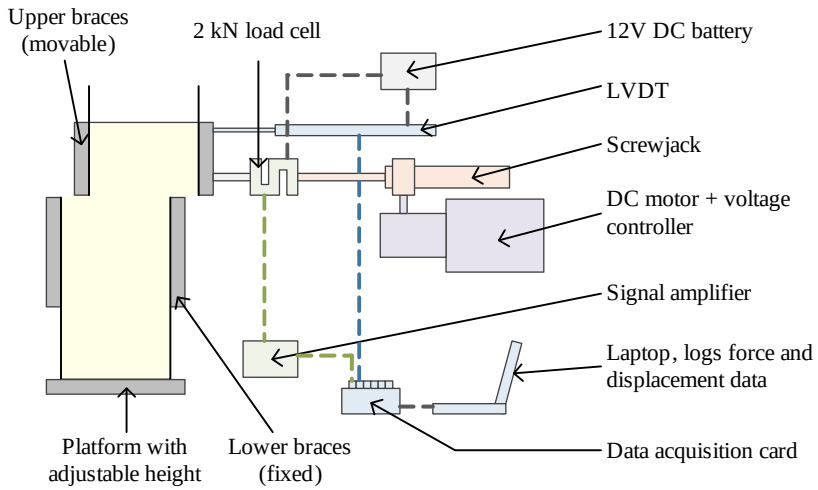

Figure 7: Schematic diagram of 150 mm dia. core direct shear set-up.

was also prepared. Each core was sheared at two or three different depths.

3 Results

3.1 Sample preparation

Dry density measurements in 32 cores showed a very constant density over a 0–275 mm depth range (Figure 8a). The best linear fit resulted in $\rho_d = (1.36 \pm 6.1 \cdot 10^{-3}) + (5.94 \cdot 10^{-5} \pm 3.73 \cdot 10^{-5}) \cdot z$ Mgm^{-3} (values of coefficients $\pm$ standard error, number of tests $n = 104$, $R^2 = 2.4\%$), where z is measurement depth [mm]. In the bottom 75 mm, the density trend (Figure 8b) was linearly increasing to $\approx$1.46 Mgm^{-3}. This increase in dry density corresponded with a decrease in water content. Gravimetric water content (w) samples taken from 33 cores showed an increasing water content over 0–275 mm depth ($w = (29.4 \pm 0.447) + (0.0142 \pm 0.00285) \cdot z$, $R^2 = 13.3\%$, $n = 162$), but below 275 mm the trend was a linearly decreasing to roughly $w = 27\%$ at the bottom.

Measured water contents and saturation levels were higher than expected based on measured water retention characteristics. Many of the outliers in water contents corresponded with fibrous and stony layers. Although this trend could be observed in dry densities as well, for successful measurements in stony soils, it was impossible to confirm for fibrous layers because it proved impossible to insert a steel core sampler without significant disturbance.

Standard penetrometer resistance (measured with the standard cone penetrometer) decreased from 0.12 MPa to 0.06 MPa with increasing depth (Figure 9). Although there were some signs of soil layering, due to the compaction procedure (50 mm thick layers), the influence on soil strength variation was small.

3.2 Blade penetrometer method

The blade penetrometer test (Figure 10) showed distinct behaviour for each core type. ABS rods showed force 'peaks' at depths where roots were present. Sudden drops in penetration resistance corresponded with rod breakages. All ABS rods broke directly below the blade penetrometer tip.

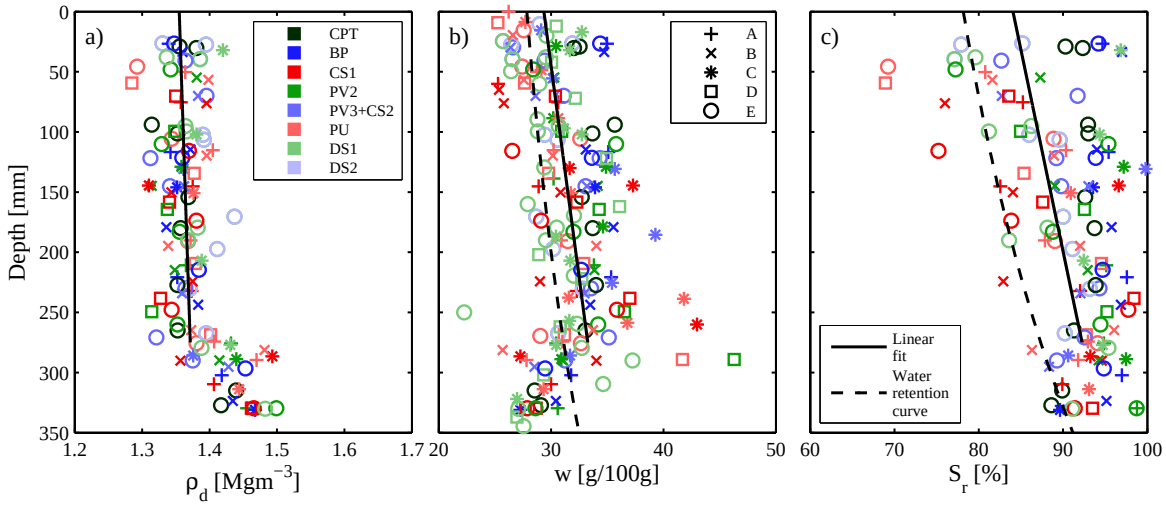

Figure 8: (a) Dry bulk densities (ρ_d), (b) gravimetric water content (w) and (c) saturation levels (S_r) for various depths in soil cores after testing. Different symbols indicate core type. Different colours indicate different preparation batches ('CPT' = cone penetration tests, 'BP' = blade penetrometer, 'CS' = corkscrew, 'PV' = pin vane, 'PU' = pull-up, 'DS' = direct shear). Solid lines represent least-squares linear fitting over the depth range. Dashed lines are based on the measured water retention characteristics described in the methods section.

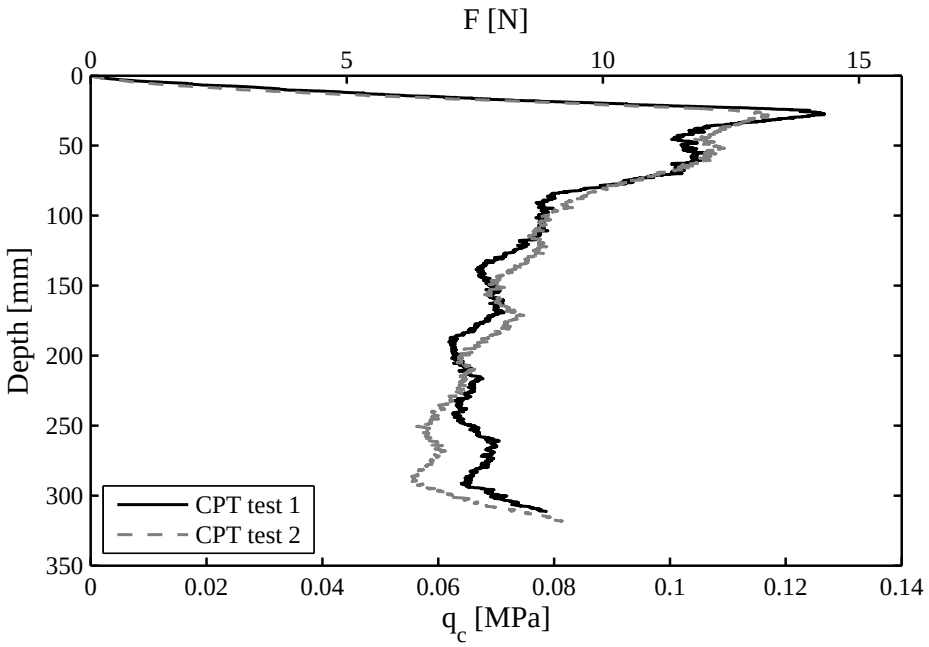

Figure 9: Standard penetrometer test results in fallow soil cores (case E).

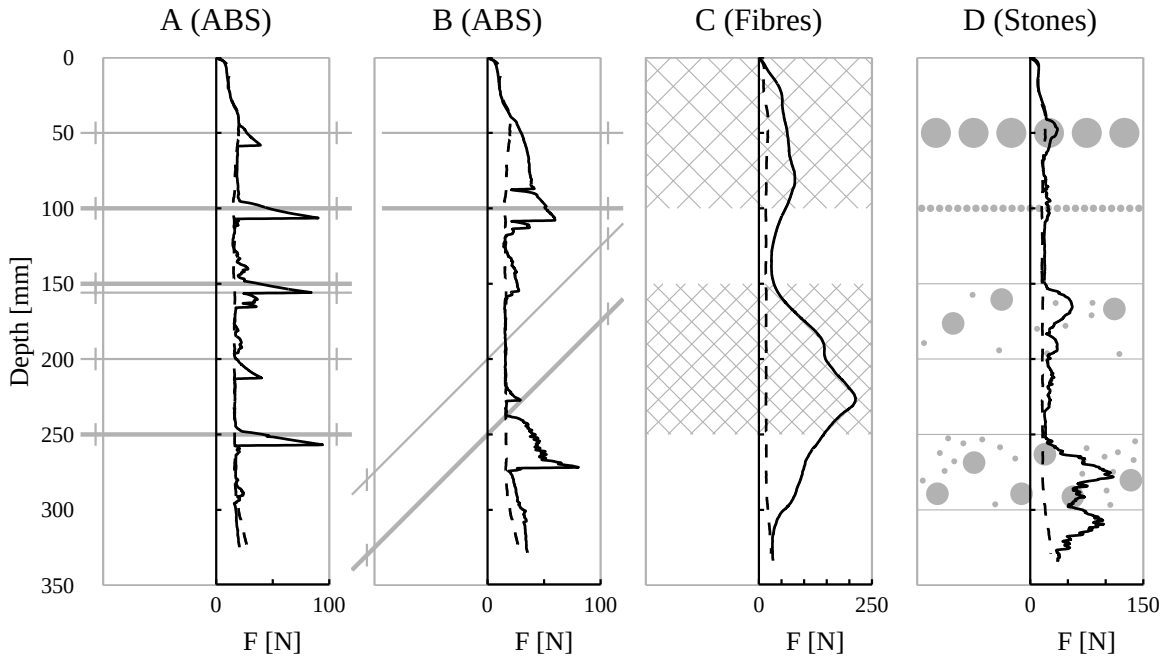

Figure 10: Blade penetrometer test results: depth plotted against installation force. In each case A–D the fallow behaviour (case E, dashed line) is plotted for reference.

The results with ABS rods show that both the penetration force increase and maximum root displacement vary with different diameters, orientation and clamping conditions. In core A, where all roots were clamped, thinner roots yielded a smaller increase in penetration resistance, with breakage occurring at higher relative displacements. In case B, the shallowest ∅1 mm root broke at much greater displacements compared with its counterpart in case A (50 and 13 mm respectively). The force-displacement gradient was much smaller for the ∅4 mm root at $z = 100$ mm in core B, and the increase in penetration resistance was much lower. This shows the importance of axial constraint on the results. The 45° roots in core B broke at lower forces than their horizontal counterparts in core A, a result which stems from either orientation or distance to anchoring point.

In contrary to ABS rods, the fibrous roots (case C) gave a large increase in force without apparent breakages. The resistance gradually built up over the first 75 of the fibrous layers. Thereafter, the resistance decreased as the blade tip penetrated deeper, even in fallow soil directly below reinforced layers.

Stones (case D) increased penetration resistance (relative to the fallow case), but, in contrast to ABS rods, there were no sudden force drops and the force-displacement behaviour was more variable. Similar to fibres, a higher stone volume fraction resulted in higher penetration resistances.

In all tests, in regions of soil where there were no inclusions, resistance approached values for tests (case E).

3.3 Pull-up method

Pull-up test results for both the installation (down, ‘dn’) and extraction (‘up’) phase are given in Figure 11. Installation resistances in cores for cases A, B and E were similar, but

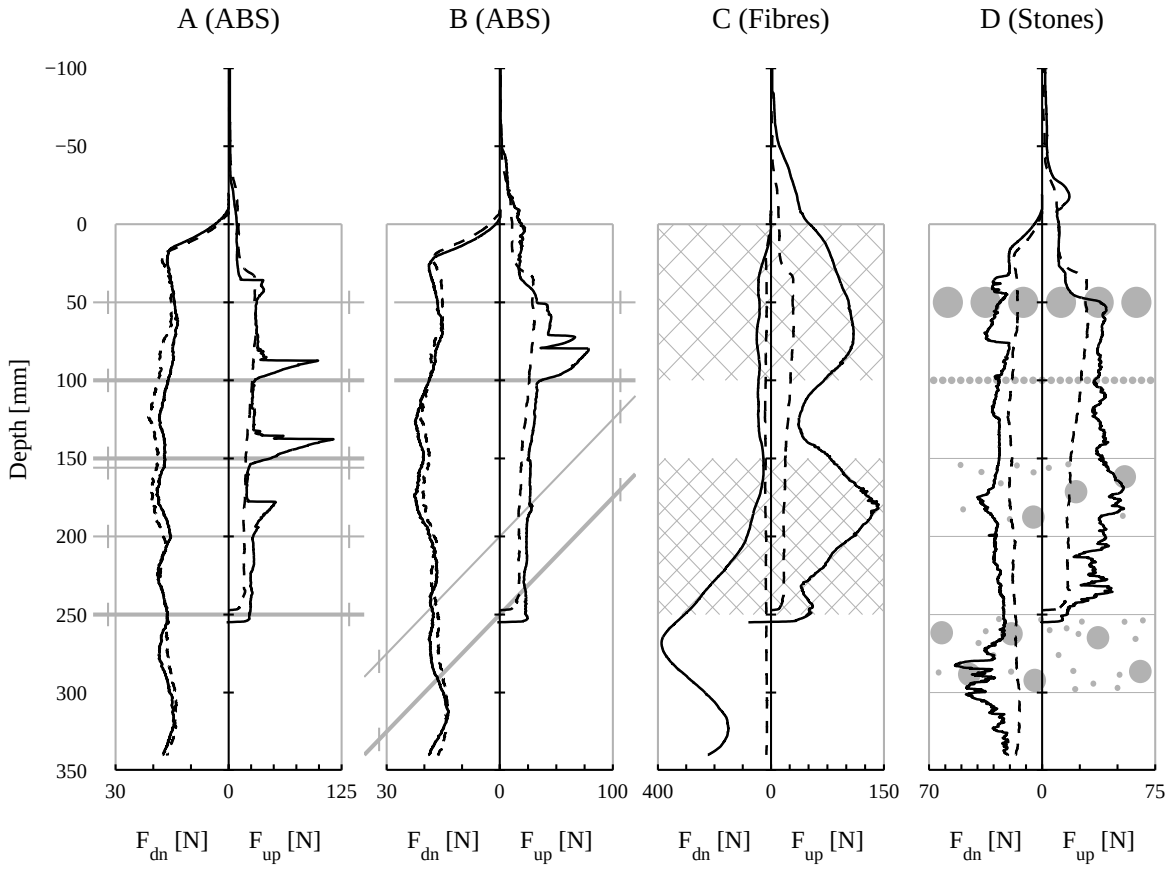

Figure 11: Pull-up device test results. For each core type, the installation force F_{dn} (left) and extraction force F_{up} (right) are plotted. Fallow results (case E) are plotted with a dashed line. For the installation phase, depth corresponds with tip depth. During extraction, depth corresponds with the depth of the wing along the central core axis.

fibres (C) and stones (D) increased the installation resistance. This resistance was much smaller than for the blade penetrometer resistance, except for in the very fibrous layer in case C ($z = 150$–250 mm).

During extraction ABS rods resulted in distinct force peaks with sudden drops in force corresponding to root breakages, similar to the blade penetrometer results. All ABS rods broke at the point of loading in case A. In case B, all rods broke apart from the top ∅1 mm rod, which slipped out. The lowest, skewed ∅4 mm rod could not be tested because it was located below the level of the expanding blade. Interestingly, the resistance during extraction in the deepest fibrous layer (case C) was not much higher than to the resistance in the top fibrous layer. The additional resistance caused by stones seemed to be small compared to blade penetrometer installation forces.

3.4 Pin vane method

Pin vane test results not only yielded root-reinforced soil peak shear strengths; rotation-shear strength traces (examples given in Figure 12) contained additional information useful to distinguish between core types. All ABS rods (case A and B) broke resulting in sudden drops in measured resistance (Figure 12a). Most rods broke at a single point within the pin

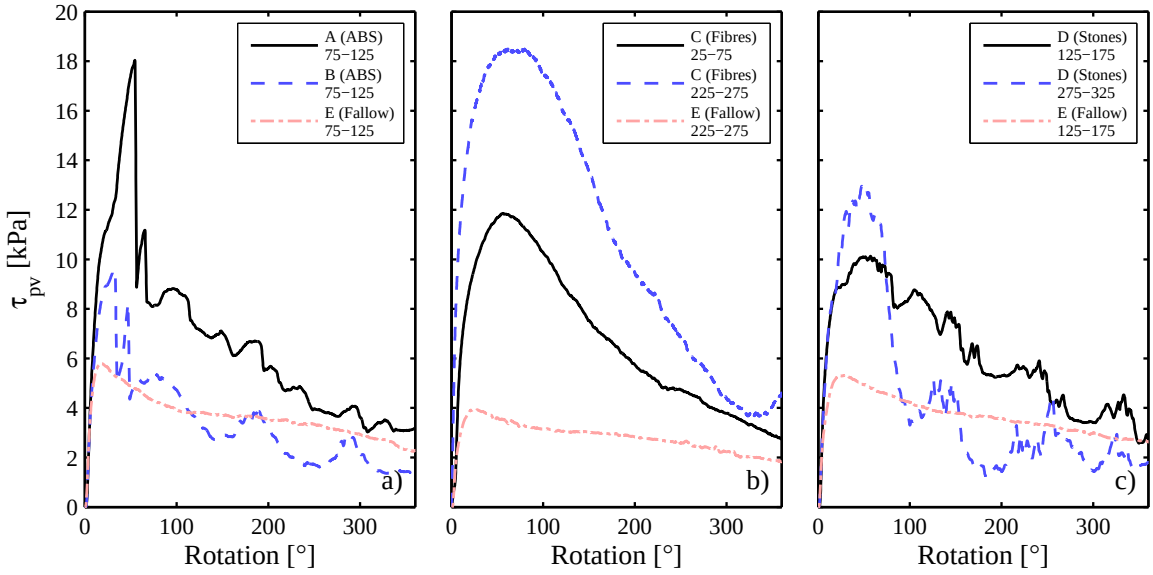

Figure 12: Example pin vane test results in cores with (a) ABS rods, (b) PP fibres and (c) stones. Core type and test depth range (in mm) are given in the keys.

vane device, though some broke at multiple points. In these six cases (out of 24), in five of them breakages were located between 14–26 mm apart, near the middle of the rod. Residual strengths were similar for fallow and ABS-rooted soil once rods had broken.

Fibrous samples (Figure 12b) showed a very smooth response with a gradual rise to peak strength and slow decline to residual strength. The lack of sudden force decrease suggested that the fibres did not break. The peak strength was much higher and occurred at higher displacements compared with the fallow soil.

Soil with stones (Figure 12c) returned very spiky force-displacement plots. Force declined more smoothly than for ABS rods. In these results, and also in test B:100mm, local maxima beyond 75° rotation lay approximately 90° apart, suggesting they were caused by the same broken root end or stone, being mobilised every time an outermost pin passes.

In most tests a cylindrical plug of soil was still trapped within the device after testing (Figure 13a). This shows that a failure mechanism occurred similar to that in standard field vane testing. In approximately a third of all tests, primarily in the wetter, deeper layers, no soil plug was extracted and the soil remained in the hole. Inspection of the hole however showed clear, round-shaped cavities where the prongs had been (Figure 13b). This suggests that the soil has rotated as an intact block with the pins rather than pins moving relative to the soil plug, again justifying the assumptions of a coring failure mechanism.

3.5 Cork screw method

Force-displacement plots for corkscrew extraction differed between core types. Extraction shear strength behaviour was similar to that in pin vane torque-rotation plots: ABS rods broke (Figure 14a), resulting in distinct force peaks. The presence of fibres (case C) resulted in ductile behaviour, with increased resistances over a large displacement range (Figure 14b). Both peak strength and displacement to failure increased with increasing fibre volume fractions. Stones (case D, Figure 14c) resulted in spiky profiles, whilst fallow (case E) soils

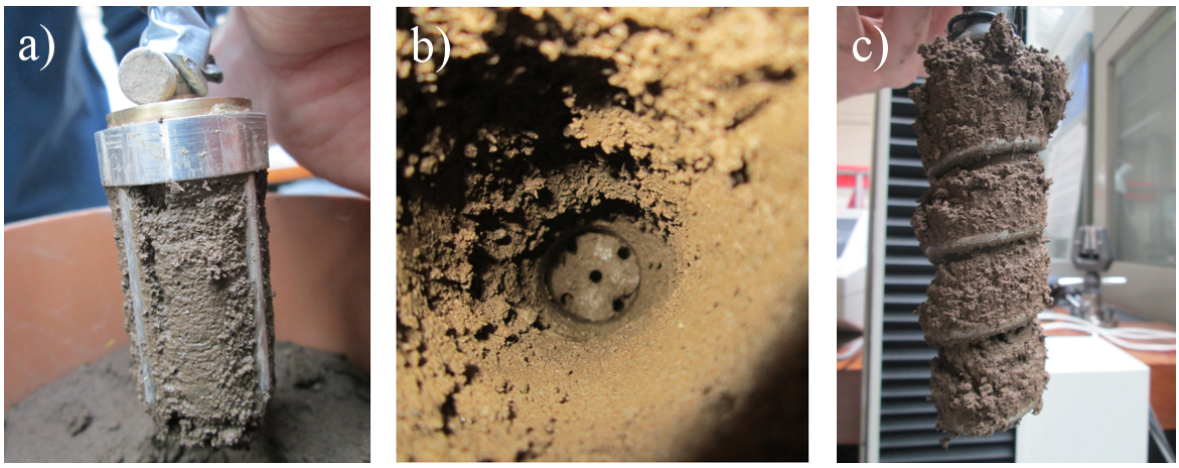

Figure 13: Soil failure mechanism: (a) pin vane with soil plug extracted; (b) pin vane with soil plug not extracted; (c) corkscrew soil plug after test at 125225 mm depth.

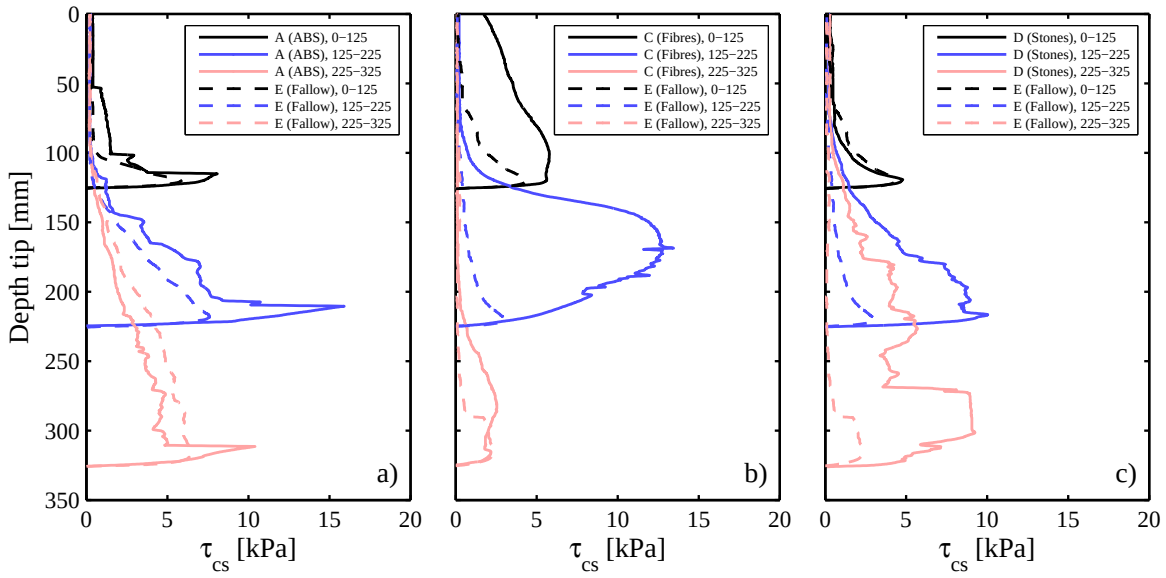

Figure 14: Example corkscrew extraction for cores with (a) ABS rods, (b) PP fibres and (c) stones. Core type and test depth range (mm) are given in the keys.

resulted in a smooth profile with lower peak displacements and a smaller width of the maximum strength peak.

Complete cylinders were extracted following almost all tests (Figure 13c), including those in deeper and wetter soil. In tests closest to the surface (z = 0–125 mm), the top of the extracted soil had a cone shape rather than a cylindrical one. This was especially pronounced in the first batch of tests, where at the top the width of the cone could be as wide as the core. The plug diameter gradually diminished with depth until z = 50 mm, where the soil plug diameter was as wide as the cork screw device. In later tests this effect was smaller, with maximum cone diameters of 90 mm observed at the top 20 mm of the soil plug. In deeper test, this effect was not observed.

An interesting feature occurred in one of the fallow test at 225–325 mm depth (Figure 14b).

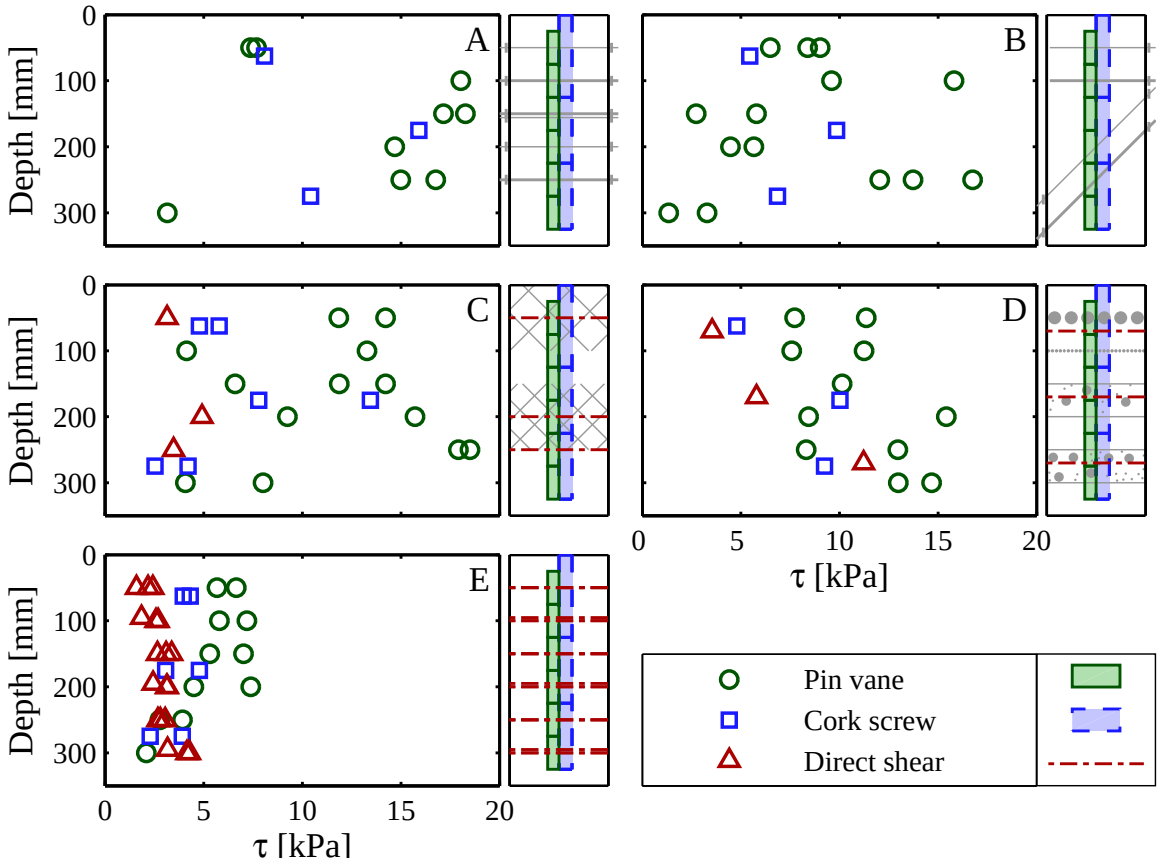

Figure 15: Peak shear strength values measured in pin vane, corkscrew and direct shear tests. Tests are sorted per core type. Per test the depth over which the shear strength is determined is indicated in the small core geometry plots. Shear strength values are averaged over test depth. Because the corkscrew device is larger than the pin vane, spatial resolution is lower and values are averaged over a larger depth range, smoothing out reinforcement effects more.

A sudden drop in force occurred after 50 mm displacement. This behaviour was observed in two other fallow tests (at 125–225 mm and 225–325 mm depth test, after extracting 20 and 35 mm respectively). It is thought this was caused by a sudden loss of suction at the void which opened up below the device during extraction. In other tests, this suction probably dissipated more gradually.

In some of the tests of the first series, higher resistances were measured because the cork screw was not inserted perfectly vertically but vertically extracted. During installation, this resulted in a sinusoidal movement with considerable amplitude in addition to the near-linearly increasing installation force, or torque, with depth. Because of this, the fallow results from this series were discarded (Figure 15). These observations show that for field applications it is important to extract the cork screw in line with the installation orientation, and also that potential misalignment can easily be observed from installation measurement torque and force.

3.6 Comparison to reference shear box testing

Direct shear tests of fibrous layers yielded greater shear strengths than in fallow tests. However, reinforcement effect was small compared to both the pin vane and cork screw methods (Figure 15). Differences may be explained by fibre orientation and test direction. During preparation fibres will be orientated mainly horizontally and therefore add less reinforcement to the horizontally oriented shear plane in the shear box tests. In pin vane and cork screw tests the shear plane was orientated vertically, resulting in more fibres crossing the shear plane at angles favourable for tensile reinforcement. Shear planes were also located close to the boundary between two soil layers. Fibre reinforcement will probably be lower at these interfaces because of fewer fibres crossing between layers, despite abrasion of the soil prior to adding a new soil layer during compaction. Shearing in cores with stones significantly increased the shear strength. Larger stone contents resulted in greater reinforcement.

Both the cork screw and pin vane tests showed decreasing strength with increasing depth in fallow soil. This trend was also observed in standard penetrometer tests (Figure 9) corresponding with decreasing suction with depth. Direct shear strengths were similar to cork screw and pin vane tests at 250–300 mm however at shallow depths they were smaller.

3.7 Quantifying root presence by blade resistance profile

In blade penetrometer and pull-up testing the best indication for the presence of individual (thicker) roots was a sudden drop in resistance. This distinct phenomenon contrasted with the gradual decrease in force, and a more noisy behaviour, associated with stick-slip between blade penetrometer and stones (case D). In field conditions, the force build-up prior to root failure may be masked by the presence of debris, variation in soil strength, overlapping of root force peaks or composite action between soil and roots as observed in fibrous experiments (case C). Linking the magnitude of sudden force decrease to root properties like diameter and strength is similarly complicated. Experiments showed increasing resistances with increases in both root diameter and axial constraint. This made it difficult to differentiate between these effects using the test method. This behaviour can be investigated further assuming ABS analogues behave as spring-supported beams (e.g. using p-y curves, Duckett (2014)). It is expected that the force-displacement response depends on the complicated interaction between root (diameter, tensile strength, bending strength), soil (resistance) and constraint characteristics (root branching, tortuosity), making careful selection of parameters and model calibration necessary.

Instead of studying the response of individual roots, the general increase in resistance compared to tests in fallow soil might be used as a proxy for soil strength. This would require similar correlations as routinely used in CPT testing to correlate tip resistance and sleeve friction to soil strength parameters. No attempts to derive such a correlation was made because of the small dataset.

Both the blade penetrometer and pull-up device are heavily dependent on reliable post-test interpretation of the data. Because these interpretations are either dependent on availability of input parameters or reliable correlations, it is concluded that these are not the most suitable methods for the desired application. However, they might prove to be a simple and useful tool for studying root occupancy as they provide information on depth of roots and an indication of their strength where incidences of breakage can be detected as a drop in force.

Although the blade penetrometer and pull-up methods employ the same mechanism and yield similar force profiles, the increased installation force and relatively low extraction force in the fibrous soil for the pull-up device suggest that installation of this device might lead to significant disturbance. Disturbance will result in a potential underestimation of root presence and reinforcement. However, compared to the blade penetrometer it will be easier to use in the field because it does not require as large a counterweight for installation and the soil itself can counteract extraction forces.

When these methods are to be adopted for measuring real roots in-situ, similar force peaks are expected as measured in tests with ABS because root strength and stiffness are similar. However, traces are likely be more difficult to interpret because of variations in root architecture (branching, orientation). Furthermore, the effect of various roots and/or debris might be superimposed, making it more difficult to quantify their individual contributions. Studies in more realistic soil and root conditions will be required to further develop these methods.

3.8 Quantifying root resistance by shear strength measurements

The presence of discrete ABS rods increased peak force with peak strength occurring at greater displacements. Sudden drops in force or torque indicated root presence, similar to the blade penetration and pull-up tests. Presence of fibrous roots (modelled with PP fibres) showed that the soil behaves in a more plastic manner with reinforcement over larger shear ranges with peak strength occurring at higher displacements.

Direct shear peak strengths are significantly lower than pin vane and cork screw results at shallow depths. This may be due to loss of suction, introduced by the slight lifting of the outer PVC core and cutting the inner plastic liner prior the direct shear test. In the time between cutting and testing (around 15 minutes) and the subsequent shearing phase (50 min. duration) negative pore pressures might have dissipated. This can explain why direct shear strengths measured at the top of samples are roughly similar to those measured lower in the core, and why the latter values are similar to those measured with pin vane and cork screw measurements at the same depth. Water contents in the samples were close to the liquid limit (w = 28–34% while w_L = 32%), so when assuming the soil behaved in an undrained fashion typical shear strengths around 1.7 kPa are expected (Wroth and Wood, 1978), similar to shear strengths measured. Secondly, in direct shear tests at 50 mm depth surface cracking was observed, suggesting a different failure mechanism and strength underestimation. Thirdly, shear rates in direct shear tests were lower than those in the other tests providing another explanation for the observed differences when rate effects are present and tests can be considered to be undrained.

In fallow soil pin vane shear strengths yielded the highest shear strengths. This was more pronounced near the surface. In cork screw tests a conical, rather than cylindrical, failure shape was observed in tests near the surface. This explains why measured shear strength using the cork screw was lower than those measured using the pin vane near the surface whilst at greater depths results were similar. In some of the pin vane tests a slight angular offset was observed resulting in a swirl of the vane around the vertical axis. Higher resistance forces were measured due to the vane being pushed through the surrounding soil rather than only mobilizing shear forces around the soil plug interface. Although the tests where this effect was obvious are discarded, it might still have influenced the remaining results to a smaller

extent.

Boundary effects might have played a role due to the relatively small diameter of the soil cores used (⌀150 mm). In pin vane tests only a 1.71 times vane diameter thick soil layer was surrounding the device and in cork screw tests the cover was 1.38 times diameter. The vicinity of the boundaries might have resulted in stiffer soil behaviour prior to reaching peak strength. The peak strength itself is not thought to be influenced because the failure mechanisms for both methods were observed to be located closely around the devices (Figure 13a,c). Only in some of the cork screw tests at 0–125 mm depth intersection between the failure surface (conical shape) and boundary was observed. In these tests peak strength is likely to be underestimated. Boundary effects could be reduced through the use of larger cores, however, due to the maximum printable length of the ABS rods (200 mm) this was not possible.

The resistance-displacement profiles, in both cork screw and pin vane tests, gave information important for landslide analysis. Only the peak strength is considered in most current analyses, e.g. when using a Mohr-Coulomb model with Bishop-circles or an infinite slope approach. However, local mobilised strength depends on local displacement, which will vary along the shear plane. The real average maximum strength over the full slide interface will therefore always be less than or equal to the average of local peak strengths. Furthermore, stress-strain behaviour affects landslide propagation. A larger area under the stress-strain curve resulting in more energy dissipation during sliding and, probably, less violent slides. Both cork screw and pin vane methods provide stress-strain information instead of only peak strength measurements. The adopted shear rates in the presented work are typical of those observed within landslides and differ to those used within in-situ shear box tests, and especially laboratory shear box tests, which are one or more orders of magnitude slower.

Intact soil cylinders observed in pin vane and cork screw tests suggest that the assumed cylindrical failure mechanisms are valid. It is likely that there is a sheared zone of soil surrounding the central cylinder due to the soil being partially saturated and containing a significant sand fraction. Fibres, or roots, increase the shear zone thickness as observed in shear vane testing of peats (Landva, 1980) and reinforced direct shear tests of sand (Jewell and Wroth, 1987; Shewbridge and Sitar, 1989). Shear strengths measured with the pin vane and cork screw may therefore be overestimated necessitating further study.

Both pin vane and cork screw devices measure root reinforcement primarily on vertical planes and therefore primarily measure the reinforcement introduced by more or less horizontally orientated roots. In landslides however the shear plane will be more horizontal, this issue can be partially addressed by inserting the measurement devices perpendicular to the root angle. Alternatively, assumptions or measurements on the distributions of root orientations can be used to verify or correct the root-reinforcement from mathematical root architecture models (e.g. Danjon et al., 2008).

Here, tests were performed in idealized conditions. Because the root analogues used had similar material characteristics as real roots, similar stress-strain patterns are expected in the field. Field trials (Meijer et al., 2015) in non-rooted soil show that both pin vane and cork screw tests yield similar results to standard field shear vane tests. Cork screw testing in soils rooted with Scots pine roots showed distinct peaks corresponding with breakage of thicker roots (diameter 2–8 mm), similar to ABS rod failures described here.

The simplicity of the equipment and the beneficial results regrading soil stress-strain

behaviour is a key advantages of the pin vane and cork screw methods. However, one downside is the need for pre-drilling of soil to prevent accumulation of root material and potential compaction prior to testing. More work is required to correlate in-situ measurement results with the strength and quantity of roots. The inclusion of root-reinforced shear tests will better assess how the proposed new methods relate to existing approaches and models.

4 Conclusion

- Four methods (blade penetrometer, pull-up, pin vane and cork screw) are developed and tested in laboratory conditions with repacked field soil at field capacity. Various inclusions were inserted to model behaviour resulting from discrete roots, fine root mats and stones within soil. All methods yield distinct behaviour when roots are present with both fibrous and thicker roots distinct from stones. Although idealised conditions, and only one soil type are considered, the results provide insight into how the devices might perform in the field.

- The blade penetrometer and pull-up method are best used for root localisation purposes. Relating measurements to soil shear strength, or root properties, requires reliable empirical correlations or the use of complicated modelling. Although the latter method can be versatile and powerful it requires many soil and root parameters which is problematic without extensive field investigation makings them less suitable for making quick and easy estimates for slope stability analysis.

- Both the cork screw and pin vane can be employed to directly measure rooted shear strengths. They can be installed without damaging the roots, yield valuable stress-strain information, are quick and easy to use, and can be performed with a mobile and light experimental set-up making them suitable for use in remote areas. Detailed follow-up study, particularly in the field, is required to validate the failure mechanisms and to correlate the measured reinforcement to root traits.

Notation

α - Van Genuchten parameter [-]
θ - Root azimuth [rad]
ρ_d - Soil dry density [Mgm^{-3}]
τ - Shear strength [kPa]
τ_{pv} - Shear strength measured with pin vane [kPa]
τ_{cs} - Shear strength measured with cork screw [kPa]
A_{tip} - Penetrometer tip surface area [mm^2]
d - Diameter [mm]
F - Penetration or extraction force [N]
H - Height [mm]
n - Van Genuchten parameter [-]
m - Van Genuchten parameter [-]
$m_{s,l}$ - Large stone mass [g]
$m_{s,s}$ - Small stone mass [g]

q_c - Penetration resistance [MPa]
S_r - Saturation [%]
$S_{r,s}$ - Maximum saturation [%]
$S_{r,r}$ - Residual saturation [%]
T - Rotational torque measured with pin vane [Nmm]
s - Soil suction [kPa]
V_f - Fibre volume fraction [%]
$V_{s,l}$ - Large stone volume fraction [%]
$V_{s,s}$ - Small stone volume fraction [%]
u - Perceived penetrometer width [mm]
u_{avg} - Average penetrometer width [mm]
w - Gravimetric water content [g/100g]
z - Depth [mm]

Acknowledgements

We are grateful to Sarah Hindmarch for her input into the development of the pin vane device, as well as to the engineering workshops at both the University of Dundee and the James Hutton Institute. G.J. Meijer acknowledges a studentship from Forest Research, funded by ClimateXChange, the Scottish Government's Centre for Expertise on Climate Change. The James Hutton Institute receives funding from the Scottish Government.

References

D. L. Achat, M. R. Bakker, and P. Trichet. Rooting patterns and fine root biomass of *Pinus pinaster* assessed by trench wall and core methods. *Journal of Forest Research*, 13(3): 165–175, 2008.

G. B. Bischetti, E. A. Chiaradia, T. Simonato, B. Speziali, B. Vitali, P. Vullo, and A. Zocco. Root strength and root area ratio of forest species in Lombardy (northern Italy). *Plant and Soil*, 278(1–2):11–22, 2005.

E. Cammeraat, R. van Beek, and A. Kooijman. Vegetation succession and its consequences for slope stability in SE Spain. *Plant and Soil*, 278(1–2):135–147, 2005.

A. J. C. Collison, M. G. Anderson, and D. M. Lloyd. Impact of vegetation on slope stability in a humid tropical environment – a modeling approach. *Proceedings of the Institution of Civil Engineers – Water Maritime and Energy*, 112(2):168–175, 1995.

E. Comino, P. Marengo, and V. Rolli. Root reinforcement effect of different grass species: A comparison between experimental and models results. *Soil & Tillage Research*, 110(1): 60–68, 2010.

N. Coppin and I. Richards. *Use of vegetation in civil engineering, CIRIA book 10*. Butterworths, Kent, 1990.

F. Danjon, D. H. Barker, M. Drexhage, and A. Stokes. Using three-dimensional plant root architecture in models of shallow-slope stability. *Annals of Botany*, 101(8):1281–1293, 2008.

M. C. R. Davies, E. T. Bowman, and D. J. White. Physical modelling of natural hazards. In Sarah Springman, Jan Laue, and Linda Seward, editors, *Physical modelling in geotechnics, ICPMG 2010*, pages 3–22, London, 2010. Taylor and Francis.

A. Diambra, E. Ibraim, D. Muir Wood, and A. R. Russell. Fibre reinforced sands: Experiments and modelling. *Geotextiles and Geomembranes*, 28(3):238–250, 2010.

B. B. Docker and T. C. T. Hubble. Quantifying root-reinforcement of river bank soils by four Australian tree species. *Geomorphology*, 100(3–4):401–418, 2008.

N. R. Duckett. *Development of improved predictive tools for mechanical soil root interaction.* PhD thesis, University of Dundee, 2014.

J. C. Ekanayake, M. Marden, A. J. Watson, and D. Rowan. Tree roots and slope stability: a comparison between *Pinus radiata* and kanuka. *New Zealand Journal of Forestry Science*, 27(2):216–233, 1997.

T. Endo. Effect of tree roots upon the shear-strength of soil. *Japan Agricultural Research Quarterly*, 14(2):112–115, 1980.

Chia-Cheng Fan and Chih-Feng Su. Role of roots in the shear strength of root-reinforced soils with high moisture content. *Ecological Engineering*, 33(2):157–166, 2008.

M. Fattet, Y. Fu, M. Ghestem, W. Ma, M. Foulonneau, J. Nespoulous, Y. Le Bissonnais, and A. Stokes. Effects of vegetation type on soil resistance to erosion: Relationship between aggregate stability and shear strength. *Catena*, 87(1):60–69, 2011.

Marie Genet, Nomessi Kokutse, Alexia Stokes, Thierry Fourcaud, Xiaohu Cai, Jinnan Ji, and Slobodan Mickovski. Root reinforcement in plantations of *Cryptomeria japonica* D. Don: effect of tree age and stand structure on slope stability. *Forest Ecology and Management*, 256(8):1517–1526, 2008.

F. Giadrossich, M. Schwarz, D. Cohen, F. Preti, and D. Or. Mechanical interactions between neighbouring roots during pullout tests. *Plant and Soil*, 367(1–2):391–406, 2013.

D. H. Gray and H. Ohashi. Mechanics of fiber reinforcement in sand. *Journal of Geotechnical Engineering (ASCE)*, 109(3):335–353, 1983.

Donald H. Gray and Robbin B. Sotir. *Biotechnical and soil bioengineering slope stabilization, a practical guide for erosion control.* John Wiley & Sons Inc, New York, 1996.

K. S. Heineck, M. R. Coop, and N. C. Consoli. Effect of microreinforcement of soils from very small to large shear strains. *Journal of Geotechnical and Geoenvironmental Engineering*, 131(8):1024–1033, 2005.

Diti Hengchaovanich and Nimal S. Nilaweera. An assessment of strength properties of vetiver grass roots in relation to slope stabilization. In *Proceedings of the International Conference on Vetiver, Chain Kai, Thailand*, pages 153–158, Bangkok, Thailand, 1996. Office of the Royal Development Projects Board.

Erdin Ibraim and Stephane Fourmont. Behaviour of sand reinforced with fibres. *Soil Stress–Strain Behavior: Measurement, Modeling and Analysis*, 146:807–818, 2007.

R. A. Jewell and C. P. Wroth. Direct shear tests on reinforced sand. *Géotechnique*, 37(1): 53–68, 1987.

D. Kim, S. Im, C. Lee, and C. Woo. Modeling the contribution of trees to shallow landslide development in a steep, forested watershed. *Ecological Engineering*, 61, Part C:658–668, 2013.

A. O. Landva. Vane testing in peat. *Canadian Geotechnical Journal*, 17(1):1–19, 1980.

T. Liang, J.A. Knappett, and A.G. Bengough. Scale modelling of plant root systems using 3-D printing. In Christophe Gaudin and David White, editors, *ICPMG2014 – Physical Modelling in Geotechnics*, volume 1, pages 361–366, Leiden, The Netherlands, 2014. CRC.

T. Liang, J.A. Knappett, and N. Duckett. Modelling the seismic performance of rooted slopes from individual root–soil interaction to global slope behaviour. *Géotechnique*, 65 (12):995–1009, 2015.

K. W. Loades, A. G. Bengough, M. F. Bransby, and P. D. Hallett. Planting density influence on fibrous root reinforcement of soils. *Ecological Engineering*, 36(3):276–284, 2010.

Z. Mao, F. Bourrier, A. Stokes, and T. Fourcaud. Three-dimensional modelling of slope stability in heterogeneous montane forest ecosystems. *Ecological Modelling*, 273:11–22, 2014.

Zhun Mao, Laurent Saint-Andre, Marie Genet, Francois-Xavier Mine, Christophe Jourdan, Herve Rey, Benoit Courbaud, and Alexia Stokes. Engineering ecological protection against landslides in diverse mountain forests: Choosing cohesion models. *Ecological Engineering*, 45:55–69, 2012.

Zhun Mao, Christophe Jourdan, Marie-Laure Bonis, Francois Pailler, Herve Rey, Laurent Saint-Andre, and Alexia Stokes. Modelling root demography in heterogeneous mountain forests and applications for slope stability analysis. *Plant and Soil*, 363(1–2):357–382, 2013.

G. J. Meijer, A. G. Bengough, J. A. Knappett, K. W. Loades, and B. C. Nicoll. Comparison of new in situ root-reinforcement measuring devices to existing techniques. In M.G. Winter, D.M. Smith, P.J.L. Eldred, and D.G. Toll, editors, *Proceedings of the 16th European Conference on Soil Mecanics and Geotechnical Engineering (XVI ECSMGE): Geotechnical Engineering for Infrastructure and Development*, pages 1621–1626, London, 2015. Institution of Civil Engineers.

R. L. Michalowski and J. Çermák. Strength anisotropy of fiber-reinforced sand. *Computers and Geotechnics*, 29(4):279–299, 2002.

S. B. Mickovski, P. D. Hallett, M. F. Bransby, M. C. R. Davies, R. Sonnenberg, and A. G. Bengough. Mechanical reinforcement of soil by willow roots: Impacts of root properties and root failure mechanism. *Soil Science Society of America Journal*, 73(4):1276–1285, 2009.

O. Normaniza, H. A. Faisal, and S. S. Barakbah. Engineering properties of *Leucaena leucocephala* for prevention of slope failure. *Ecological Engineering*, 32(3):215–221, 2008.

J. E. Norris. Root reinforcement by hawthorn and oak roots on a highway cut-slope in southern England. *Plant and Soil*, 278(1–2):43–53, 2005.

J. E. Norris and J. R. Greenwood. Field measurements in geomechanics. In F. Myrvoll, editor, *Field Measurements in Geomechanics: Proceedings of the 6th International Symposium, Oslo, Norway, 23–26 September 2003*, pages 593–597. CRC Press, 2003.

Joanne E. Norris, Alexia Stokes, Slobodan B. Mickovski, Eric Cammeraat, Rens Van Beek, Bruce C. Nicoll, and Alexis Achim. *Slope stability and erosion control: Ecotechnical solutions*. Springer, Dordrecht, The Netherlands, 2008.

V. Operstein and S. Frydman. The influence of vegetation on soil strength. *Ground Improvement*, 4:81–89, 2000.

Mandy Pohl, Dominik Alig, Christian Koerner, and Christian Rixen. Higher plant diversity enhances soil stability in disturbed alpine ecosystems. *Plant and Soil*, 324(1–2):91–102, 2009.

N. Pollen and A. Simon. Estimating the mechanical effects of riparian vegetation on stream bank stability using a fiber bundle model. *Water Resources Research*, 41(7):W07025, 2005.

N. Pollen-Bankhead and A. Simon. Enhanced application of root-reinforcement algorithms for bank-stability modeling. *Earth Surface Processes and Landforms*, 34(4):471–480, 2009.

N. Pollen-Bankhead and A. Simon. Hydrologic and hydraulic effects of riparian root networks on streambank stability: Is mechanical root-reinforcement the whole story? *Geomorphology*, 116(3–4):353–362, 2010.

B. Reubens, J. Poesen, F. Danjon, G. Geudens, and B. Muys. The role of fine and coarse roots in shallow slope stability and soil erosion control with a focus on root system architecture: a review. *Trees-Structure and Function*, 21(4):385–402, 2007.

Mary M. Riestenberg. *Anchoring of thin colluvium by roots of sugar maple and white ash on hillslopes in Cincinnati, US Geological Survey Bulletin 2059-E*. US Government Print Office, Washington, US, 1994.

M. Schwarz, P. Lehmann, and D. Or. Quantifying lateral root reinforcement in steep slopes – from a bundle of roots to tree stands. *Earth Surface Processes and Landforms*, 35(3): 354–367, 2010.

S. E. Shewbridge and N. Sitar. Deformation characteristics of reinforced sand in direct shear. *Journal of Geotechnical Engineering (ASCE)*, 115(8):1134–1147, 1989.

Alexia Stokes, Joanne E. Norris, L. P. H. Van Beek, Thom Bogaard, Erik Cammeraat, Sloban B. Mickovski, Anthony Jenner, Antonino Di Iorio, and Thierry Fourcaud. How vegetation reinforces soil on slopes. In J. E. Norris, A. Stokes, S. B. Mickovski, E. Cammeraat, R. Van Beek, B. C. Nicoll, and A. Achim, editors, *Slope stability and erosion control: Ecotechnological solutions*, pages 65–118. Springer, 2008.

Alexia Stokes, Claire Atger, Anthony Glyn Bengough, Thierry Fourcaud, and Roy C. Sidle. Desirable plant root traits for protecting natural and engineered slopes against landslides. *Plant and Soil*, 324(1–2):1–30, 2009.

Chaosheng Tang, Bin Shi, Wei Gao, Fengjun Chen, and Yi Cai. Strength and mechanical behavior of short polypropylene fiber reinforced and cement stabilized clayey soil. *Geotextiles and Geomembranes*, 25(3):194–202, 2007.

L. P. H. Van Beek, J. Wint, L. H. Cammeraat, and J. P. Edwards. Observation and simulation of root reinforcement on abandoned Mediterranean slopes. *Plant and Soil*, 278(1–2):55–74, 2005.

M. Th. Van Genuchten. A closed-form equation for predicting the hydraulic conductivity of unsaturated soils. *Soil Science Society of America Journal*, 44(5):892–898, 1980.

L. J. Waldron. Shear resistance of root-permeated homogeneous and stratified soil. *Soil Science Society of America Journal*, 41(5):843–849, 1977.

L. J. Waldron and S. Dakessian. Soil reinforcement by roots – calculation of increased soil shear resistance from root properties. *Soil Science*, 132(6):427–435, 1981.

Zhengquan Wang, Dali Guo, Xiangrong Wang, Jiacun Gu, and Li Mei. Fine root architecture, morphology, and biomass of different branch orders of two Chinese temperate tree species. *Plant and Soil*, 288(1–2):155–171, 2006.

C.P. Wroth and D. M. Wood. The correlation of index properties with some basic engineering properties of soils. *Canadian Geotechnical Journal*, 15(2):137–145, 1978.

T. H. Wu and A. Watson. In situ shear tests of soil blocks with roots. *Canadian Geotechnical Journal*, 35(4):579–590, 1998.

T. H. Wu, W. P. McKinnell III, and D. N. Swanston. Strength of tree roots and landslides on Prince of Wales Island, Alaska. *Canadian Geotechnical Journal*, 16(1):19–33, 1979.